Supplementary Information Figures

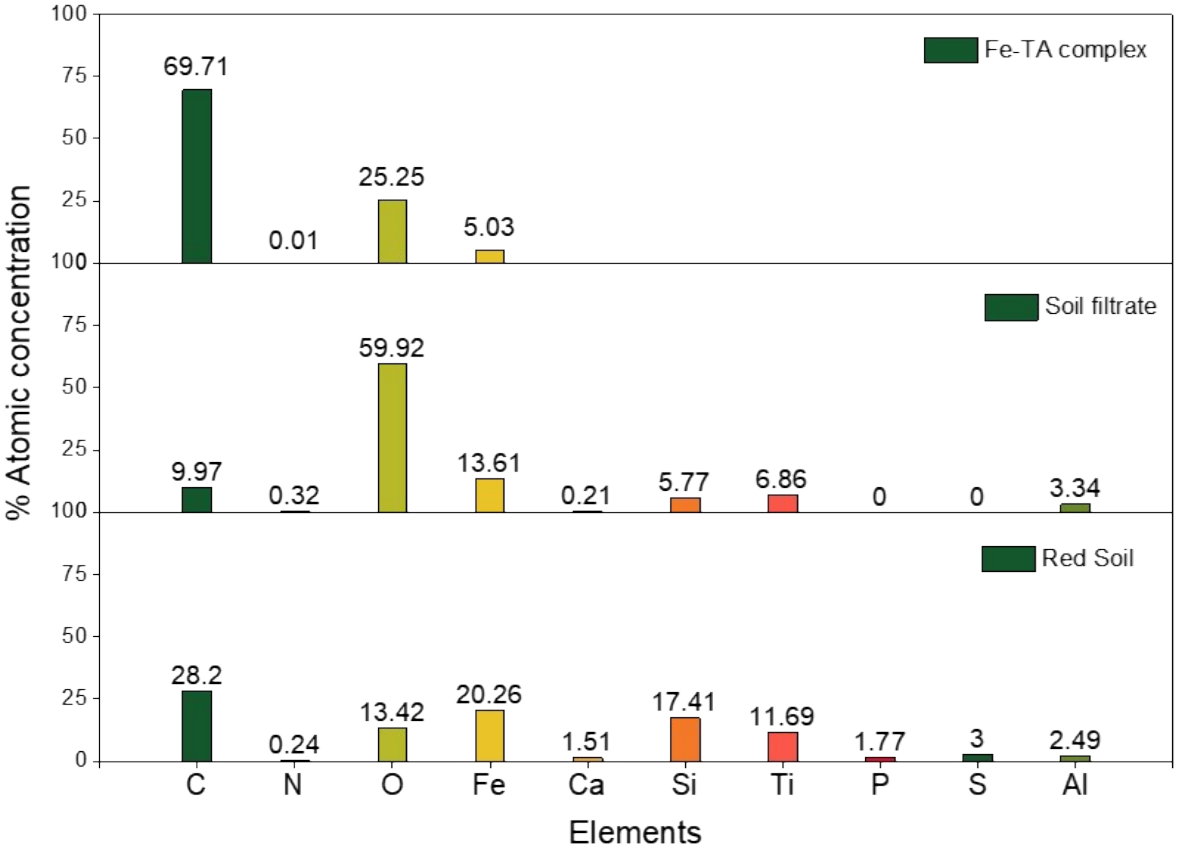

Figure S1. Quantification of XPS survey of Fe-TA complex (Black PPT), Soil filtrate and Red Soil (from top to down).

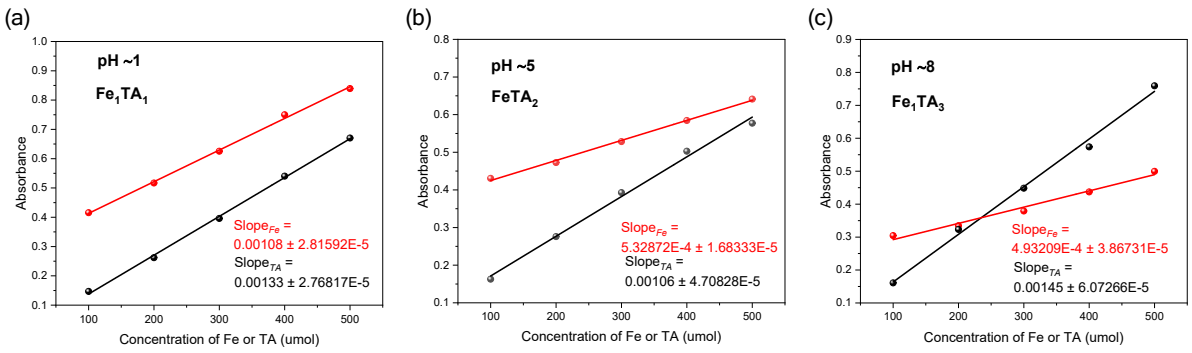

Figure S2. Slope-ratio UV–Visible analysis for determining the coordination stoichiometry of Fe–tannic acid complexes at different pH values (pH 1, 5, and 8). The linear fitting slopes were used to determine the formation of FeTA, $FeTA_2$, and $FeTA_3$ species.

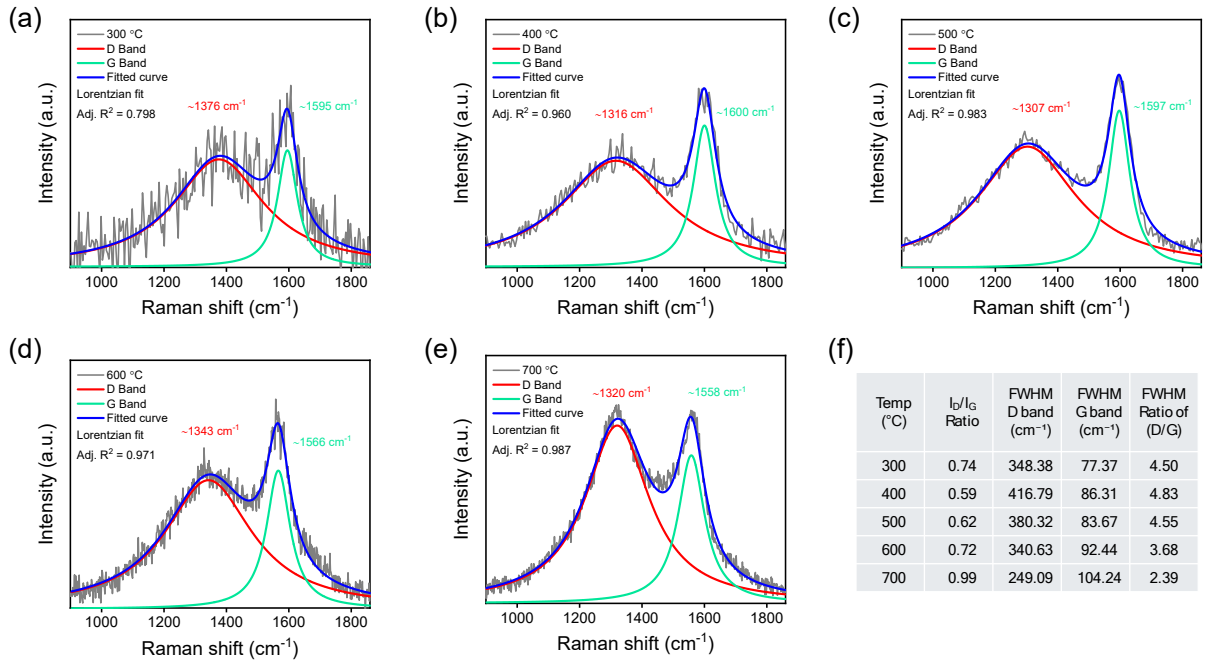

(f)

Temp (°C)	I_D/I_G Ratio	FWHM D band (cm^{-1})	FWHM G band (cm^{-1})	FWHM Ratio of (D/G)
300	0.74	348.38	77.37	4.50
400	0.59	416.79	86.31	4.83
500	0.62	380.32	83.67	4.55
600	0.72	340.63	92.44	3.68
700	0.99	249.09	104.24	2.39

Figure S3. Raman spectral deconvolution of Fe-TA precursor pyrolyzed at temperatures ranging from 300 to 700 °C. Each spectrum was deconvoluted into the D band (red, ~1307–1376 cm^{-1}, disordered carbon) and G band (green, ~1558–1600 cm^{-1}, graphitic sp^2 carbon), with cumulative fit in blue and raw data in grey. Key parameters are summarized in the inset table.

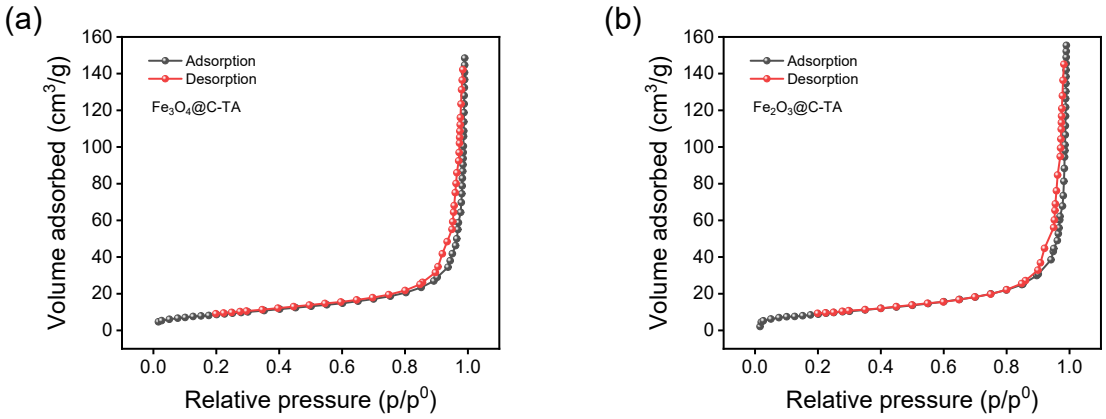

Figure S4. Nitrogen adsorption-desorption isotherm curves of (a) Fe_2O_3@C-TA, (b) Fe_3O_4@C-TA.

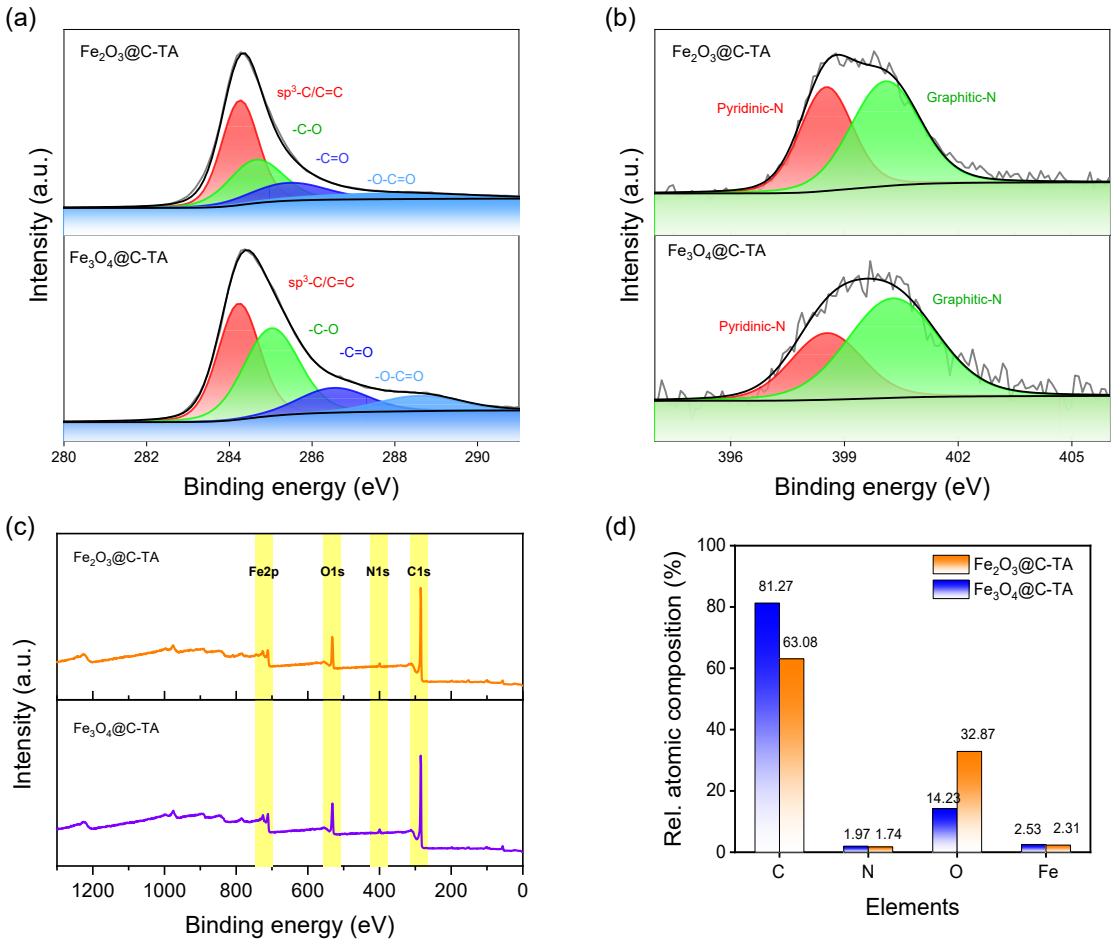

Figure S5. (a) High-resolution C 1s XPS spectra of both catalysts showing sp^2-C, C–N/C=N and O–C=O components. (b) High-resolution N 1s spectra of both catalysts displaying pyridinic-N/Fe–N, pyrrolic/amine-N and graphitic-N/Fe–N species. (c) XPS survey spectra confirming the presence of C, N, O and Fe elements. (d) Relative atomic composition derived from XPS analysis for both samples.

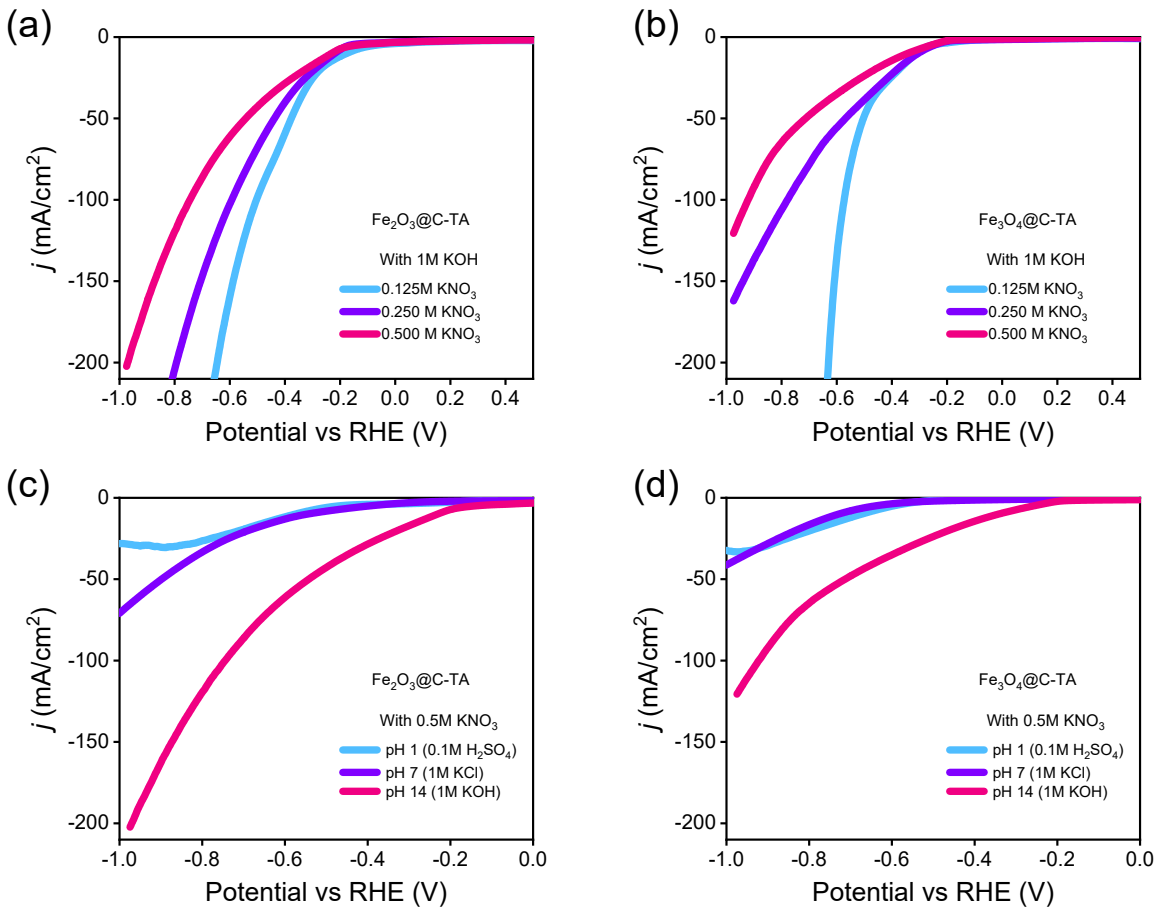

Figure S6. LSV curves in 1 M KOH containing varying KNO_3 concentrations (0.125 M, 0.25 M, and 0.5 M) with 1 M KOH as supporting electrolyte of (a) Fe_2O_3@C-TA and (b) Fe_3O_4@C-TA electrodes; LSV curves at varying pH conditions for (c) Fe_2O_3@C-TA and (d)Fe_3O_4@C-TA electrodes, demonstrating enhanced NO_3RR activity and steeper cathodic current response at pH 14 (1 M KOH).

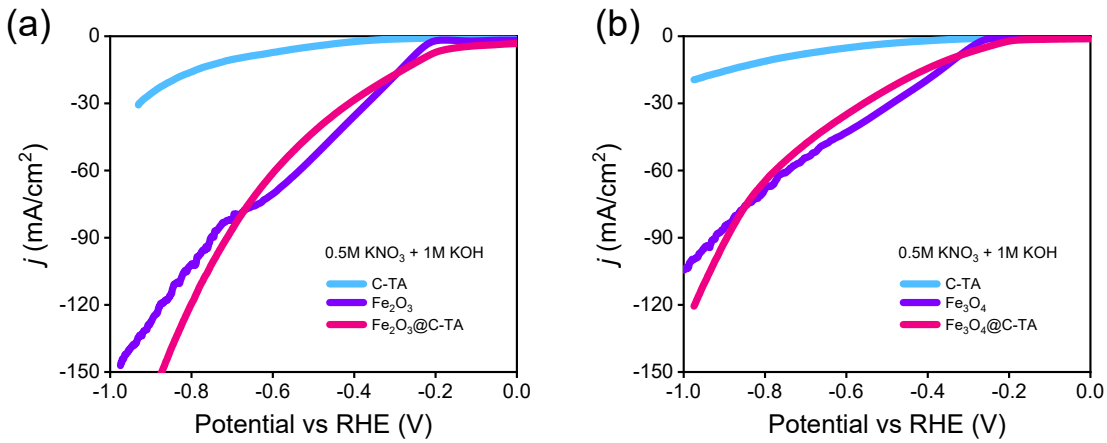

Figure S7. LSV curves in 0.5 M KNO_3 + 1 M KOH electrolyte of C-TA, Fe_2O_3, and Fe_2O_3@C-TA electrodes (a), and C-TA, Fe_3O_4, and Fe_3O_4@C-TA electrodes (b), where Fe_2O_3 or Fe_3O_4 and C-TA were individually studied to elucidate their respective contributions to the enhanced NO_3RR activity observed for the Fe_2O_3@C-TA or Fe_3O_4@C-TA composites respectively.

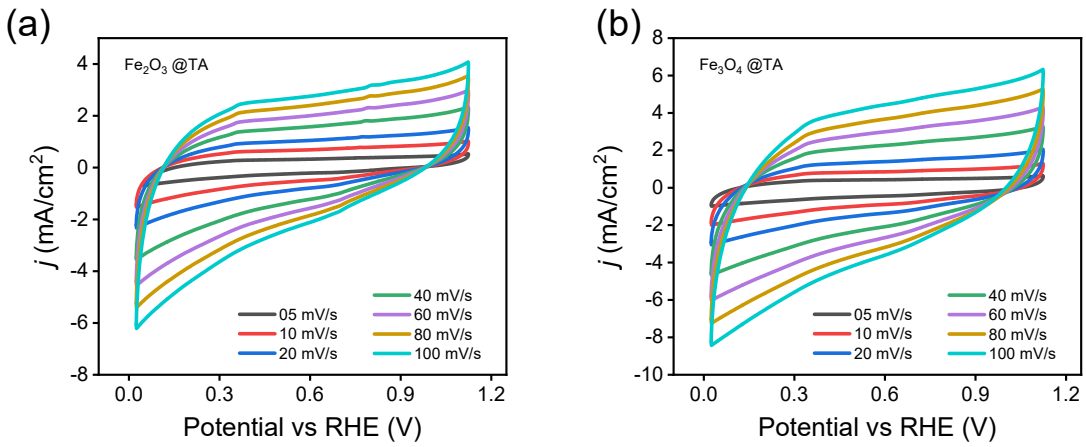

Figure S8. Cyclic voltammetry plots: (a) Fe_2O_3@C-TA, and (b) Fe_3O_4@C-TA in non-faradaic region for calculating C_{dl} and electrochemical surface area (ECSA) taking C_s = 50 µF/cm^2.

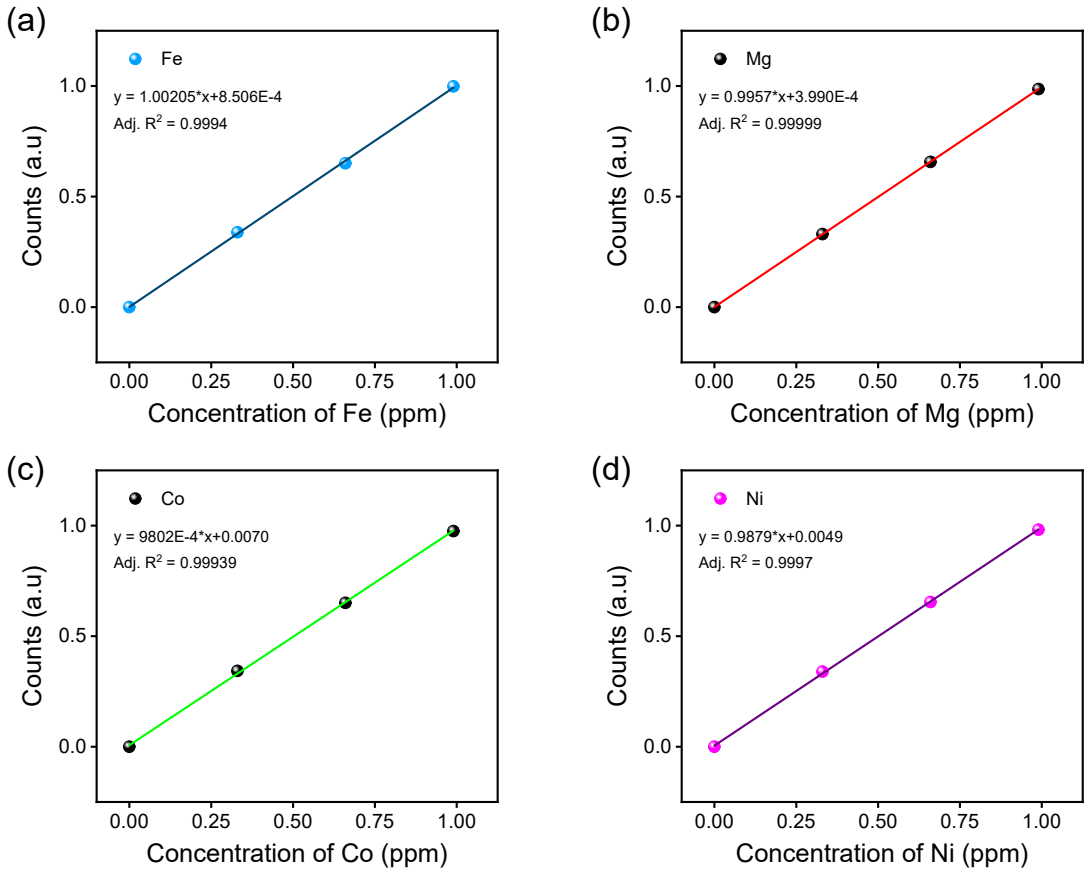

Figure S9. Calibration curve utilised for ICP-MS quantification of (a) Fe, (b) Mg, (c) Co and (d) Ni metals.

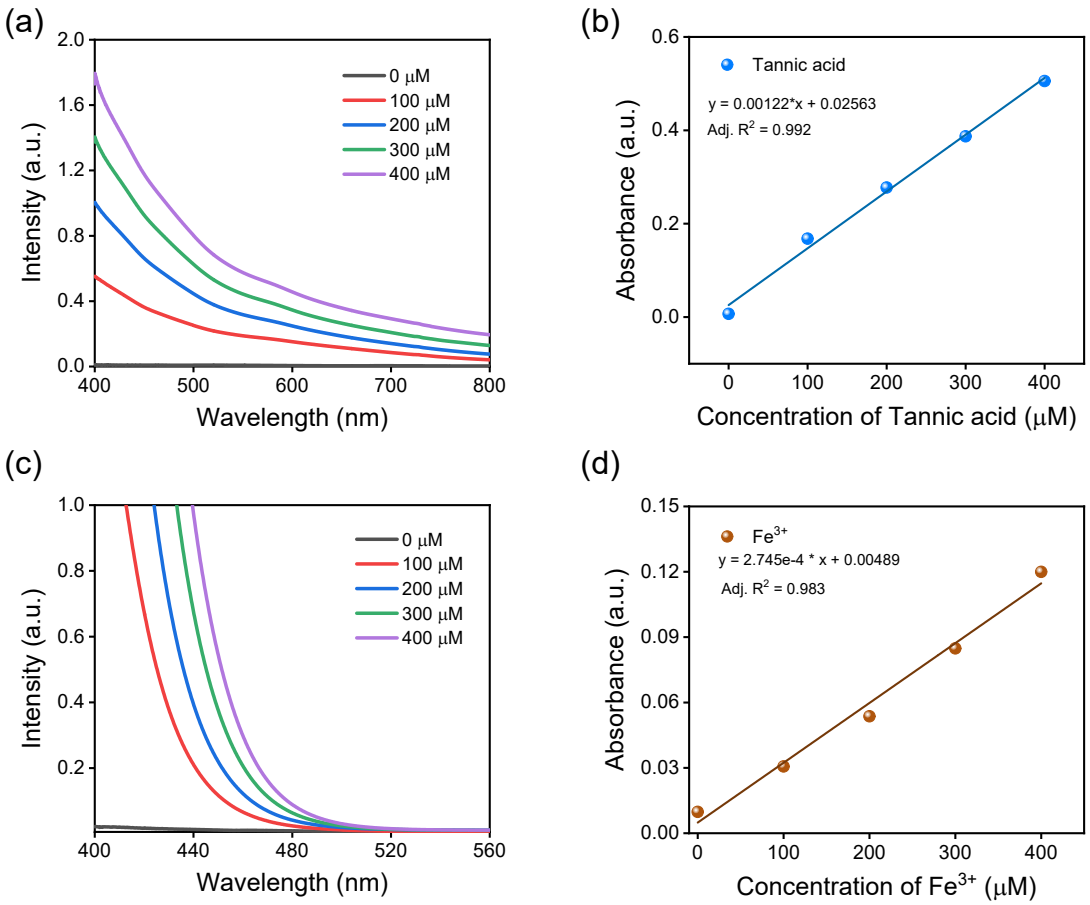

Figure S10. UV-Visible calibration curves used for quantification of (a) Tannic acid and (b) Fe^{3+}.

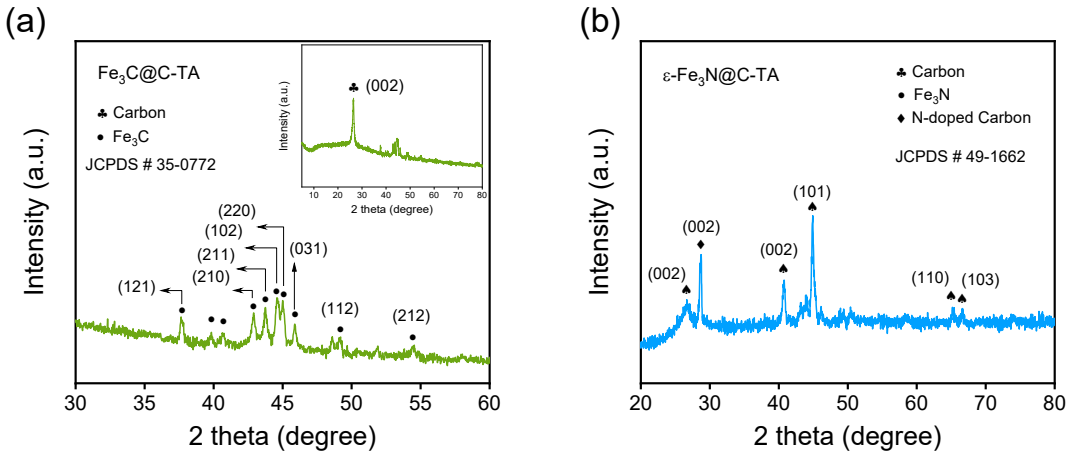

Figure S11. XRD spectra showing the phase-pure synthesis of (a) Fe_3C@C-TA and (b) Fe_3C@C-TA via catalyst portfolio.

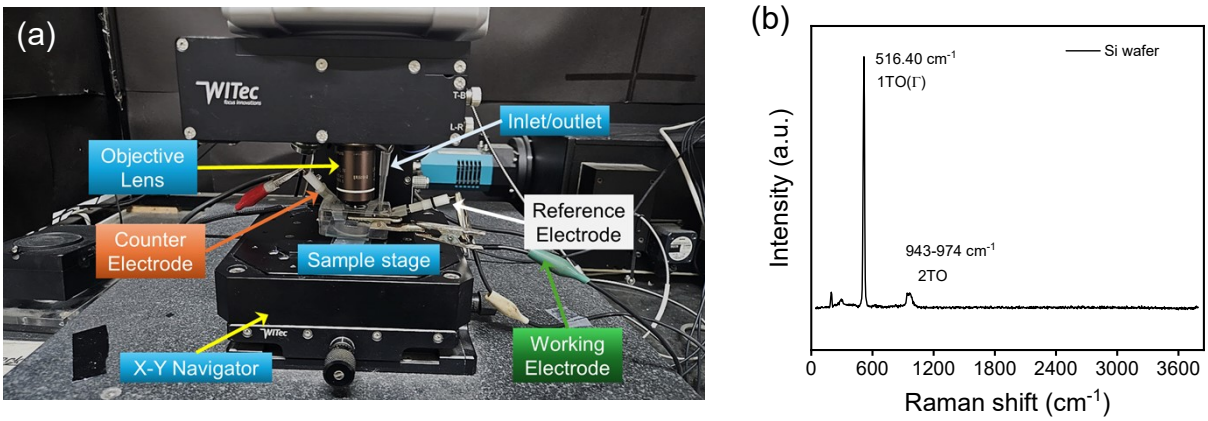

Figure S12. (a) Custom-designed *in situ* Raman set up and (b) The Si(100) wafer taken for Raman peak calibration; 1TO(Γ) peak at 516.40 cm^{-1} confirms accuracy and reference of spectrometer.

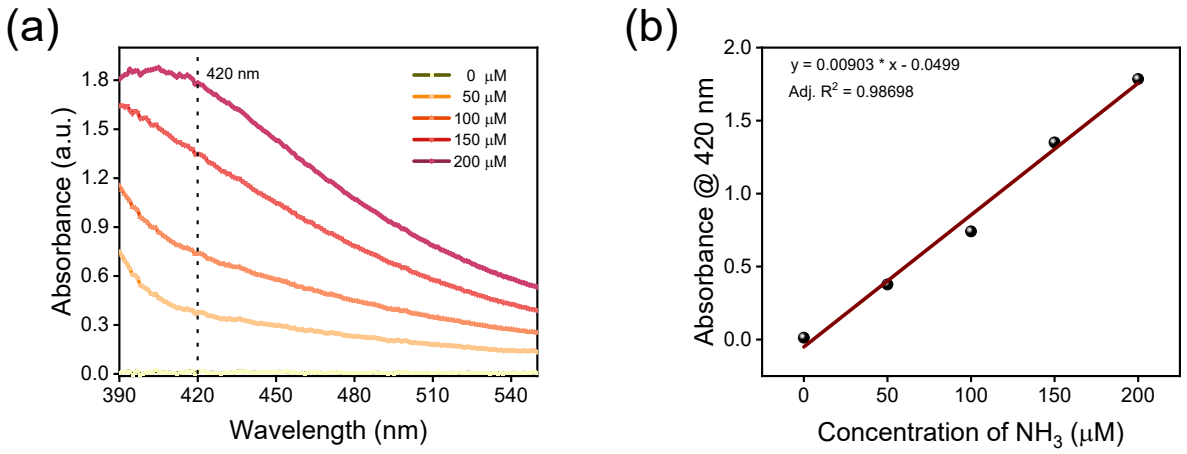

Figure S13. UV–visible spectrophotometric calibration curve of NH_4Cl for NH_3 quantification using Nessler's reagent.

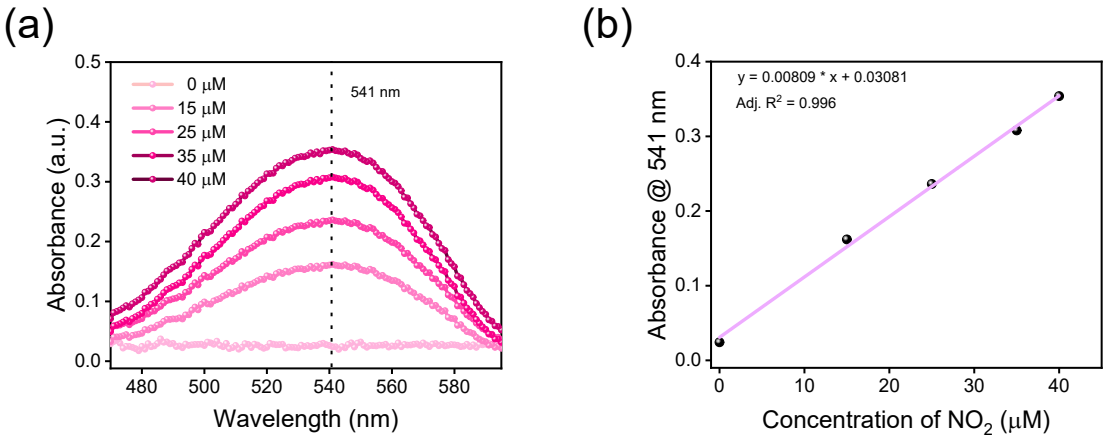

Figure S14. UV–visible spectrophotometric calibration curve of KNO_2 for NO_2^- quantification using Griess reagent.

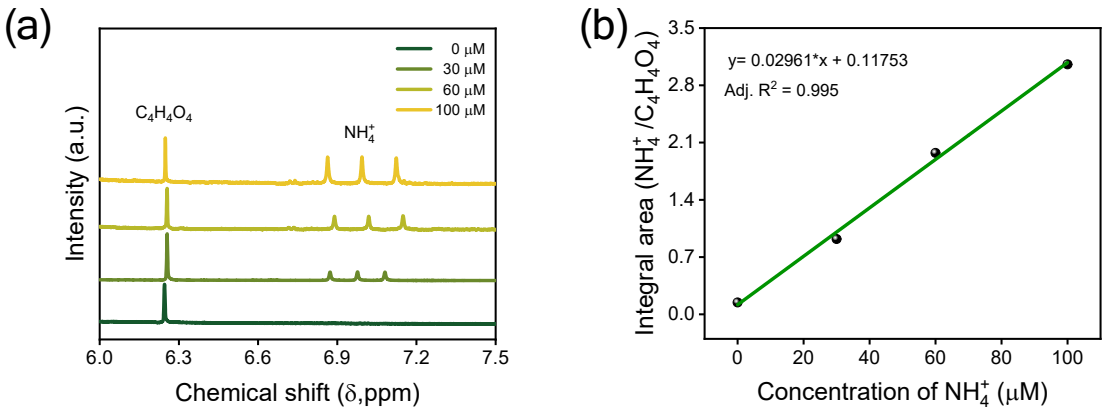

Figure S15. ^{1}H-NMR spectrophotometric calibration curve of NH_4Cl for NH_4^+ quantification.